Chapter 6

Parametric Pulse Shaping

This chapter introduces parametric pulse shaping with linearly polarized pulses and applies them on NaK (isotope) optimization experiments. The next chapters will treat a parameterization of polarization shaped pulses.

6.1 Introduction

Performing coherent control experiments with a pulse shaper usually brings along the problem of finding a solution in a nearly unimaginably huge search space. For a phase and amplitude shaper with N pixels, this space has a dimensionality of $2N$. Therein, the number of possible solutions are indeed enormous, they amount to $P^{2N} = 10^{768}$ for the SLM-256[1], or even $1750^{1280} \approx 10^{4151}$ for the SLM-640[2]. Despite the fact that evolutionary algorithms are supposed to be in their element when treating highly complex problems, differing runs for free optimization regularly show different results to various degrees. If a reliable problem inversion is desired, one can not, for many cases, get around reducing the complexity to a comprehensible level. Therefore, a reduction of the number of optimization parameters in order to reduce search space size seems to be a logical way. Realities represented by the search space might not be physically feasible and can be excluded. Another approach is to omit certain possibilities for inquisitive purposes, like deliberately finding solutions in a restricted regime. Such restrictions allow to choose a framework for the algorithm to work in, it becomes possible to "ask" the experiment certain questions, which it tries to answer via the closed feedback-loop procedure by finding an optimized Hamiltonian in the redefined search space.

6.2 Historical perspective

Since the development of pulse shapers capable of modulating the spectral phase $\phi(\omega)$, a number of ways of parametrizing it were thought of.

[1] having $P = 1000$ different voltage settings within the mandatory 2π retardance range

[2] because the higher number of pixels (N=640) are even more highly resolved, due to a reduced modulation depth of only 4π instead of 7π at 770 nm, while having the same 12-bit resolution as the SLM-256 (with 128 pixels)

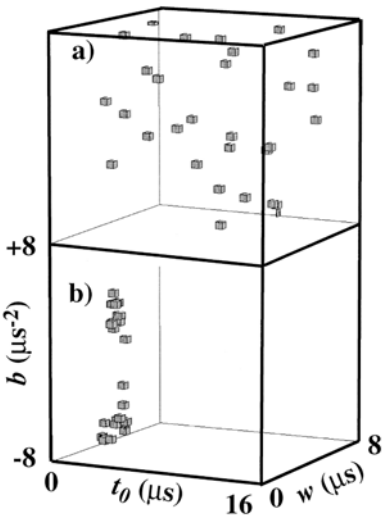

Figure 6.1: Three-parametric search space encoding of a single pulse. The small cubes represent the individual's solutions at (a) the first generation, and (b) after 17 iterations, having agglomerated to two niches. Taken from Ref. [114].

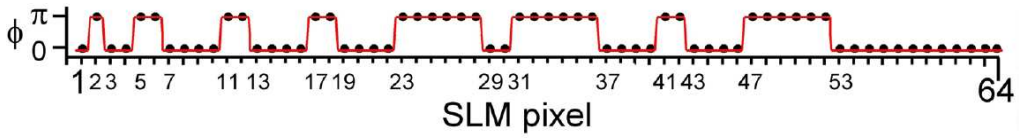

Figure 6.2: Phase pattern with π steps used for binary shaping (taken from Ref. [116])

AOM parameters. The first parametric optimization, to the authors knowledge, was performed by Bardeen et al. in 1997, who used a parametrization of the radio frequency of the arbitrary waveform generator of an acousto-optical modulator like [114]

$$V_{RF}(b, t_0, w) = A \exp\big(-\frac{(t-t_0)^2}{w^2} + ib(t-t_0)^2 + ic(t-t_0)^3\big). \tag{6.1}$$

The parameters were the amplitude A, time center of the Gaussian window t_0 (which corresponds to the central frequency of the pulse), the width w (which determines the spectral width), the linear chirp b and the quadratic chirp c. Their test sample was the IR125 laser dye molecule and the goal was to transfer population from the ground to the first excited state. They visualized the progress of the optimization 3D space for three selected parameters. Fig. 6.1 (a) displays the population distribution at the first generation and (b) at the 17^{th} generation, where a (parallel) convergence towards two promising niches can be seen.

Combining pixels/phase discretization. In order to reduce search space, combining neighbouring SLM pixels to a single control value can help not only determining the frequency-resolution dependence of the problem (and as a side-effect, even reduces temporal complexity [66]) but also improves convergence speed and robustness under noise. In Ref. [115], a phase discretization reduced 1000 voltage steps to a manageable few and provided comparable results with no significant decrease in performance for the observed system.

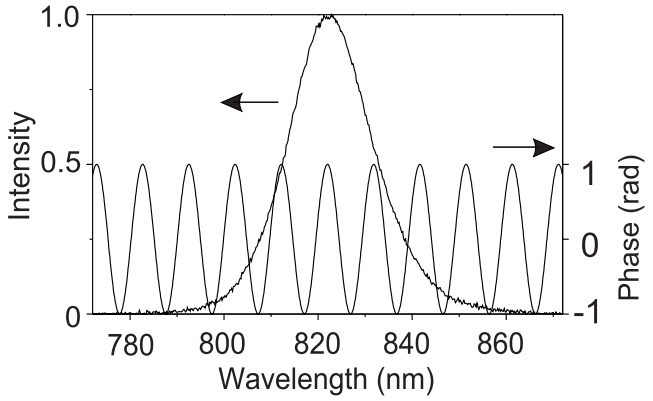

Figure 6.3: Periodic phase parametrization to create bright and dark pulses in Cs. Taken from Ref. [59].

Binary phase. A special type of step size reduction is "binary phase shaping" (see Fig. 6.2), introduced by the Dantus group [116, 117] for applications in two-photon microscopy, with a clear focus on reliability, convergence speed, and simplicity.

Periodic phase functions. The first application of a phase encoding with periodic functions was for non-resonant two-photon interactions between atomic energy levels of caesium, parametrized by

$$\phi(\omega) = \alpha \cos(\beta\omega). \tag{6.2}$$

Using this function (Fig. 6.3) caused an enhancement or cancellation of the two-photon transition probability by interference effects with so-called bright and dark pulses. Periodic phase functions were applied for various systems, starting with bright/dark pulses with atomic sodium [113], ionization of NaK molecules [26], to more complex biological systems, like the light-harvesting antenna complex LH2 from Rhodopseudomonas acidophila which is a photosynthetic purple bacterium [118]. In another application, the pulse trains created by a periodic phase function were employed to reduce the requirements of nonlinear CARS (Coherent Anti-Stokes Raman Scattering) microscopy to a single source (single-pulse CARS) [119]. A study of the complexity reducing capacities of parametric shaping was conducted by Bartelt et al. [26] using symmetrical pulse trains that were created by a sine parametrization

$$\phi(\omega) = a \cdot \sin\left(\Omega(\omega) + C\right) \tag{6.3}$$

that also incorporated Taylor terms such as

$$\Omega(\omega) = \tau(\omega - \omega_0) + a_2(\omega - \omega_0)^2 + a_3(\omega - \omega_0)^3 + \cdots \tag{6.4}$$

where the parameters τ and a_2 control the distance and the linear chirp, respectively. Figure 6.4 displays the XFROG trace a pulse form generated by such a phase function.

Polynomial phase. Another variant is a polynomial phase encoding

$$\phi_n = \sum_k c_k \Big(\frac{n - N_0}{N}\Big)^k \tag{6.5}$$

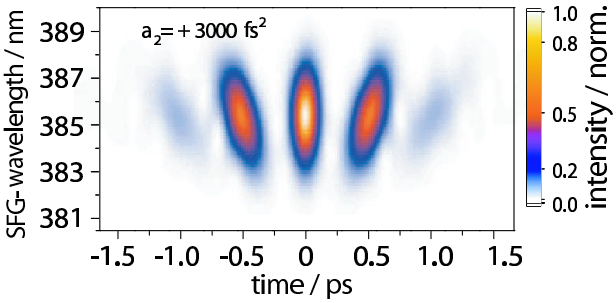

Figure 6.4: XFROG traces of pulses generated by a sine-parametrization like Eq. 6.3, with different Taylor terms from Eq. 6.4. Taken from Ref. [36].

with n as the pixel number, N_0 the pixel offset, N the number of pixels, k the maximum order, and c_k as the Taylor coefficients. The first, straightforward application was re-compression of a femtosecond pulse that had travelled through a glass fiber [115], compensating for the time-stretching caused by group velocity dispersion [120]. A polynomial phase encoding was also recently used optimizing the ground state vibrational dynamics of polymers [121] and for selective spectral filtering of vibrational modes of β-carotene in solution [122].

Triangular phase. Similarly as a linear spectral phase shifts one pulse's envelope in time, a triangular spectral phase generates a double pulse with different central frequencies in time [123] as

$$\phi(\omega) = \mathrm{sgn}\left[\omega - (\omega_0 + \delta\omega)\right]\frac{\Delta\tau}{2}\left[\omega - (\omega_0 + \delta\omega)\right], \tag{6.6}$$

with $\Delta\tau/2$ as the triangular phase slope connected to half the pulse separation and $(\omega_0 + \delta\omega)$ as the division point, which determines spectral width and amplitude. Such double pulses were utilized in Ref. [124] for determining fitness landscapes of the solvated dye molecule IR140.

Table 6.1 contains an overview of spectral phase parametrizations in the literature including the systems applied. The "temporal parametrization" from the bottom of the list will be discussed next in more detail.

6.3 Temporal parametrization

A temporal parametrization looks at pulse generation in a different way as spectral phase parametrization: It does not ask what the result of a specific phase pattern will be in the time domain; it constructs a desired waveform in the time domain and then tries to realize it by calculating an adequate spectral phase filter. A prominent example is a double pulse in the time domain, which is a known concept from pump-probe spectroscopy [30, 31], where the distance of two sub pulses is varied while, for example, a wavepacket propagation on potential energy surfaces of molecules is studied.

An early time-domain representation [75] describes a double pulse sequence[3] of two sub pulses with the envelope $F(t)$ and the phases φ as

[3] see also Eq. 2.15

parametrization	**system**	**bibliography**	**year**
single pulse	dyes in solution	Bardeen et al. [114]	1997
combine pixels	SHG	Zeidler et al. [115]	2001
reduce phase steps	SHG	Zeidler et al. [115]	2001
binary phase shaping	SHG	Comstock et al. [116]	2004
	phosphite & pyridine	Pastirk et al. [117]	2005
polynomial phase	pulse re-compression	Zeidler et al. [115]	2001
	K_2	Hornung et al. [75]	2000
	polydiacetylene	Zeidler et al. [121]	2006
	β-carotene	Konradi et al. [122]	2006
periodic phase	atomic Na	Zeidler et al. [115]	2001
	atomic Cs	Silberberg et al. [59]	1998
	LH2	Herek et al. [118]	2002
	NaK	Bartelt et al. [26]	2002
	single pulse CARS	Dudovich et al. [119]	2002
triangular phase	optical investigations	Renard et al. [123]	2004
	IR140	Vogt et al. [124]	2006
temporal	atomic Na	Hornung et al. [113]	2000
	K_2	Hornung et al. [75]	2000
Legendre, Hermite	*suggested*	Shir et al. [125]	2006

Table 6.1: Overview of phase parametrizations in optimal control experiments.

$$E(t) = e^{i\omega_0 t} F(t) e^{i\varphi_1} + e^{i\omega_0 t} F(t-\tau) e^{i\varphi_2} \tag{6.7}$$

and was employed to the one-photon (3s $\rightarrow$ 3p) transition for atomic Na. The population created by such a pulse was calculated in Ref. [126] to be proportional to

$$|c_2|^2 \propto \cos\left(\phi_1 - \phi_2 + \delta\omega \cdot \tau\right) \tag{6.8}$$

where $\delta\omega$ was the detuning from the (3s $\rightarrow$ 3p) transition.

6.3.1 Parametric pulse form calculation

For the temporal parameterization presented in this thesis, a complex electrical field is constructed by overlaying N sub pulses, which can be performed either in the time or frequency domain.

Spectral Domain. Superposing (adding) the complex electrical fields $E_1(\omega)$, $E_2(\omega)$, $\cdots$ $E_N(\omega)$ to obtain $E_{out}(\omega)$ can be written as

$$E_{out}(\omega) = \sum_N E_N(\omega). \tag{6.9}$$

Each E_N can be expressed by a generating (input) pulse $E_{in}(\omega)$ times an individual filter function $\tilde{H}_N(\omega)$ like

$$\tilde{H}_N(\omega) = R_N \cdot e^{i\phi_N(\omega)} \tag{6.10}$$

whereby ϕ_N is constructed using the Taylor terms from Eq. 2.24; and the constant R_N is used to steer the amplitude (shape) of the sub pulse. R_N^2 is also proportional to the relative[4] sub pulse energy. The linear phase b_1 will then be responsible for the temporal (envelope) shift of the respective sub pulse, etc. The resulting field can be written as

$$E_{out}(\omega) = E_{in}\tilde{H}_1 + E_{in}\tilde{H}_2 + \cdots + E_{in}\tilde{H}_N = E_{in} \cdot \sum_N \tilde{H}_N(\omega). \tag{6.11}$$

The frequency dependent filter $\tilde{H}(\omega)$ can be calculated by dividing

$$\tilde{H}(\omega) = \frac{E_{out}(\omega)}{E_{in}(\omega)} = \sum \tilde{H}_N(\omega) = R(\omega) \cdot e^{i\phi(\omega)} \tag{6.12}$$

whereby $T(\omega) = |R(\omega)|^2$ becomes the transmission and $\phi(\omega)$ the phase filter/retardance to be written on the pulse shaper in order to obtain such a composite pulse.

If the generating sub pulses are not chosen with power restrictions in mind, the transmission $T(\omega)$ might exceed the value of one at some points. This is physically infeasible, as a pulse shaper can only diminish, not amplify any frequency component. Therefore, a normalization of $T(\omega)$ by finding the maximum

[4] relative because an eventual normalization, described later

$$T_{norm}(\omega) = \frac{T(\omega)}{\max T(\omega)} \tag{6.13}$$

has to be performed, reducing[5] the total output power to $1/\max\ T(\omega)$. The pulse form in the time domain $E_{out}(t)$ can then be obtained by inverse Fourier transformation.

Time domain. Similarly, temporal sub pulse fields in the time domain $E_1(t), E_2(t)$ etc. can be superposed using the same formalism stated above, just by substituting $t \rightarrow \omega$, yielding the temporal phase "filter" $\phi(t)$ (like Eq. 2.18), the Taylor coefficients a_n (Eq. 2.19), and the impulse response $\tilde{h}(t)$. The impulse response can be Fourier transformed as [66]

$$\tilde{H}(\omega) = \int \tilde{h}(t) e^{-i\omega t}\ dt \tag{6.14}$$

in order to yield the corresponding spectral filter function $\tilde{H}(\omega)$, to be eventually normalized, and then applied to the pulse shaper.

6.3.2 Double pulse examples

The effect of polynomial, spectral Taylor phase functions on single pulses in the time and frequency domain have already been pictured in Refs. [36, 71].

To emphasize the to-be-introduced implementation into an evolutionary algorithm, an overview for asymmetrical double pulses[6] will be presented (Fig. 6.5). The two columns to the right depict what to write on the shaper in order to obtain the two left columns, or the other way around: what the filter function (right) would have to look like in order to obtain the temporal and spectral traces on the left. The columns from left to right are: SFG-CC (calculated using Eq. 3.5), spectral intensity (including the spectral resolution[7] using Eq. 3.4), transmission $T(\omega)$ (normalized), and the phase filter $\phi(\omega)$.

Fig. 6.5 displays for six examples, what happens or what is required when one sub pulse of a double pulse is modified by a spectral phase filter or by a change in relative energy R_1^2/R_2^2. The red/gray lines are a reference $\Delta t = 200$ fs double pulse and the black curves depict the deviation when changing the respective parameters.

b_1**.** The first row shows a temporal sub pulse shift from t=200 fs to t=400 fs for the second sub pulse, which corresponds to different modulations of the pulse spectra. For double pulses, the temporal distance Δt can also be assessed from the modulation frequency $\Delta\nu = 1/\Delta t$ of the transmission pattern.

[5] when performing systematic measurements like pump-probe scans with a pulse shaper, such a normalization has to be taken into account

[6] which will be frequently used in this and the following chapters

[7] 0.55 nm

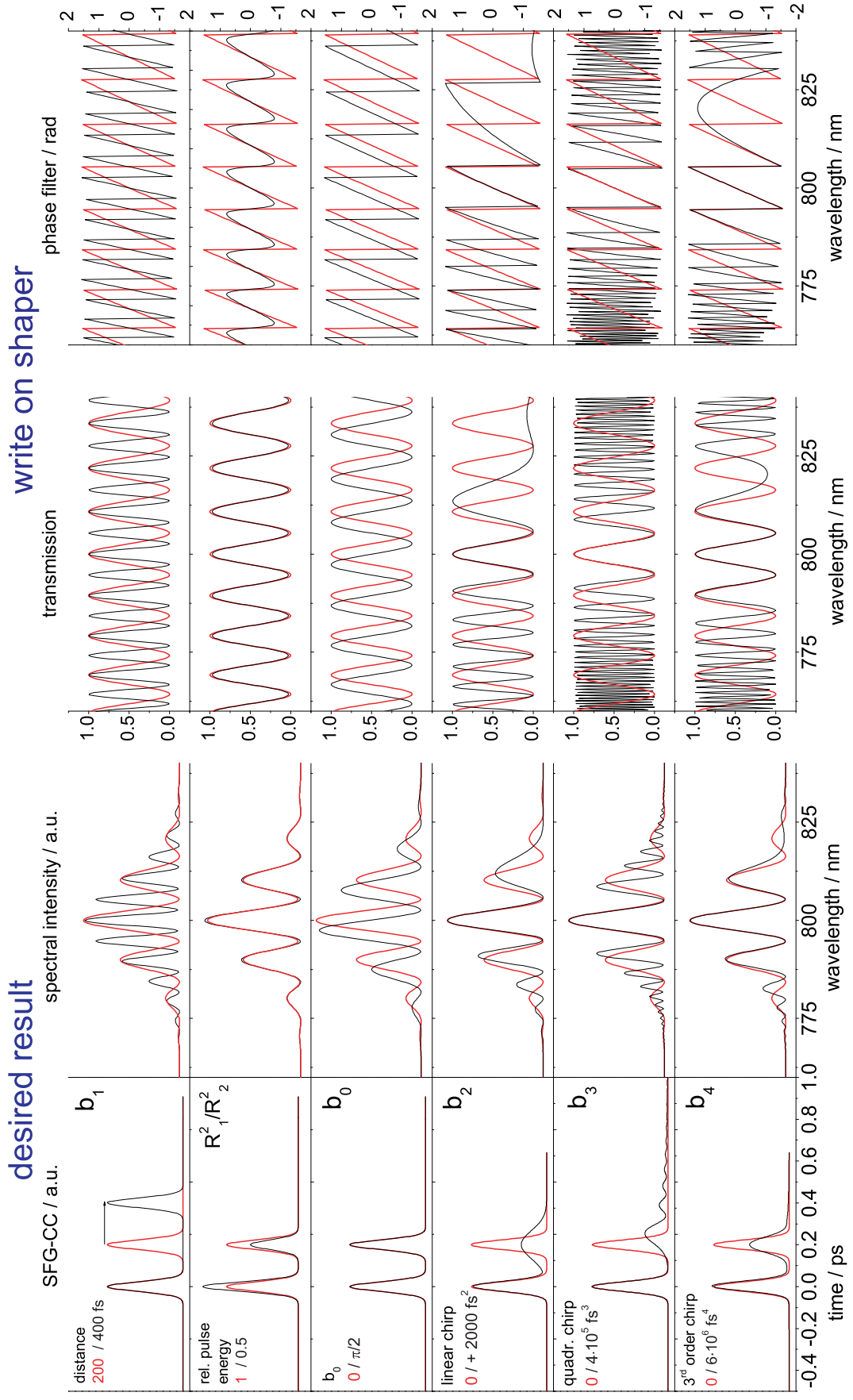

Figure 6.5: Double pulse parametrization overview.

R_1^2/R_2^2**.** The second row shows the impact of an energy-ratio change by choosing a different $R_1^2/R_2^2 = 2:1$ instead of the reference's 1:1. For this case, the spectra and transmission patterns are barely changed[8]. The deciding feature that causes the temporal redistribution is the phase filter, which is straightened towards higher energy ratios.

b_0**.** Shifting the electrical field below the envelope (zero order phase) has no impact on the SFG-CC, but can be measured as a frequency shift of the spectral intensity modulation where the central frequency will no longer constitute the most prominent peak, as in the b_0=0 case. When $b_0 = \pi/2$ for the pulse at t=200 fs, both transmission and phase filter are shifted by the same "phase" amount[9].

b_2, b_3, b_4**.** The impact of chirp is presented in the last three rows with a linear, quadratic, and cubic example. The linearly chirped, second sub pulse (b_2=+2000 fs^2) has a reduced maximal temporal intensity, but the same sub pulse energy. The spectra show a distinct asymmetry, with a higher modulation "frequency" at the lower wavelength end. A quadratic chirp of $b_3 = 4{\cdot}10^5$ fs^3 for one sub pulse creates a characteristic tail in time and has symmetric spectra, a third order chirp of $b_4 = 6{\cdot}10^6$ fs^4 creates an offset in the baseline in time and an asymmetric spectrum.

6.3.3 Algorithm implementation

The above stated parameter set can be incorporated in an objective variable $\vec{x}$ for N sub pulses with spectral Taylor terms up to the order of M as

$$\vec{x} = \left\{b_{0,0}, b_{0,1}, \cdots, b_{M,N}, R_1^2, \cdots, R_N^2\right\} \tag{6.15}$$

whereby $b_{m,n}$ is the m-th order phase of the n-th sub pulse. Internally, the employed algorithm rescales the (in principle) arbitrary boundary conditions to the interval [0,1]. This has the advantage that a single-step size mutational rate adaptation, which acts equally on all scaled parameters, can be employed. This speeds up convergence noticeably, as no second-degree parameters (such as parameter specific mutation rates [40]) have to be included and self-adapted. When more than two sub pulses are encoded, the linear phase b_1 (position in time) is substituted by a sub pulse distance Δt_n, counting from the sub pulse that occurs at earliest times.

$$\vec{x} = \left\{b_{0,0}, \Delta t_n, \cdots, b_{M,N}, R_1^2, \cdots, R_N^2\right\} \tag{6.16}$$

That way, not only one parameter can be saved, but also, if the distance between the first and second sub pulse changes, the temporal positions of sub pulse three and higher are adapted etc., which is reasonable from an experimental point of view when applied on a molecular excitation scheme. Otherwise, the standard algorithm settings, as described in Sec. 2.4, and depicted in Fig. 2.2 were used.

[8]The spectra would converge to a Gaussian when one pulse disappears, as no more interference occurs.

[9]This has the advantage that for example different vibrational transitions can be addressed by such spectral patterns.

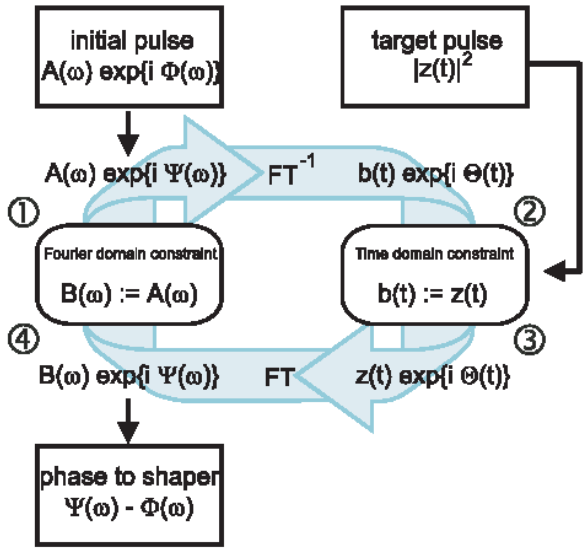

Figure 6.6: Iterative algorithm to generate predefined pulses in phase-only mode (taken from Ref. [129]).

6.3.4 Phase-only shaping

Although the calculation of compound pulse forms (Eqs. 6.9 to 6.12) has to be conducted using phases and amplitudes, the parametric NaK optimization experiments of this chapter were performed with phase-only shaping in order to keep the total pulse power constant during the run to guarantee fair conditions of consecutive pulse shapes, as amplitude modulation always goes hand-in-hand with a change in total power, depending which frequencies have to be diminished to obtain particular pulse shapes. There are only numerical methods to determine a phase filter function which approximates a given intensity or cross-correlation profile without amplitude modulation except for trivial cases. The first work calculating such phase filter functions were Ref. [127], followed by Ref. [128], where an experimental feedback was implemented to fit a measured waveform to the desired.

A fast and reliable way using the Gerchberg-Saxton algorithm [130] was presented in Ref. [129] (see Fig. 6.6) and was used for the experiments[10]. The algorithm iteratively calculates spectral phases and adapts them to the desired temporal shape using a combination of simplex downhill [132] and simulated annealing [47] methods.

6.3.5 Three-pulse NaK optimization

The "temporal" experiments were performed with the Tsunami oscillator with the SLM-256 at a central wavelength of 780 nm and a spectral bandwidth of 6.4 nm. Compared to the free optimization experiments presented in earlier chapters, now, a distinct reduction of the search space is exercised, and only three sub pulses are allowed to propagate in order to ionize the NaK molecule.

From the available parameters, the sub pulse distance, their energy, zero order phase, and linear chirp were used, spanning (only) an eleven-dimensional[11] search space; consequently the convergence speed was much faster, with no experiment

[10] implemented in the *Lab2* [131] program package, available from the authors of Ref. [129]
[11] $3 \times 4 - 1$ (only two distances)

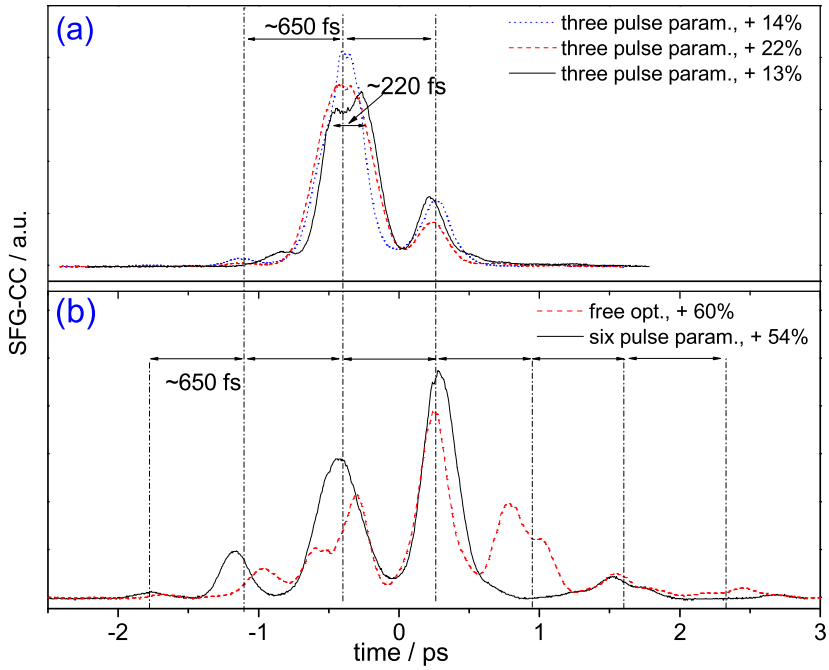

Figure 6.7: SFG-CC traces of three optimized pulse shapes from (a) a three- and (b) a six-pulse parametrization. The dashed line in (b) is the result from free, phase-only optimization.

requiring more than a few minutes. To avoid sub pulse overlaps with the given temporal pulse length of approx. 150 fs, the distances were encoded to [180,2000] fs. For the other parameters: [1:1,1:10] was allowed for the energies ratios, [-20000,20000] fs^2 for the linear chirps, and $[-\pi, \pi]$ for the zero order phases b_0.

The SFG cross-correlations of three experimental runs are plotted in Fig. 6.7 (a). For all cases, a prominent double pulse structure can be seen with another closely spaced double pulse embedded within the major pulse. The distances of the major features amount to approximately 650 fs, which corresponds to $1.5 \cdot T_{osc}$ of a wavepacket in the first excited $A(2)^1\Sigma^+$ state.

To demonstrate the reliability and reproducibility of parametric shaping and see how the parameters evolve in the newly defined search space, a course analysis of the three runs is performed. Fig. 6.8 shows how the parameters converge, with an outstanding case (middle column, + 22% ionization efficiency improvement compared to the unshaped pulse) and two sub-optimal results (left and right column, +14% and +13%, respectively).

The top row displays the XFROGs of the three results, which are quite coincidental in shape, so the differences in optimization factor must therefore result either from small variations, or from features the XFROG does not reveal, such as zero order phases. The broad pulse around t=0 fs actually consists of two sub pulses, which have a distance of about 200 fs, which is close to the resolution limit of the employed bandwidth. The second row shows the development of the distances, which show a slow increase for (a) towards the final values. For the other cases, the

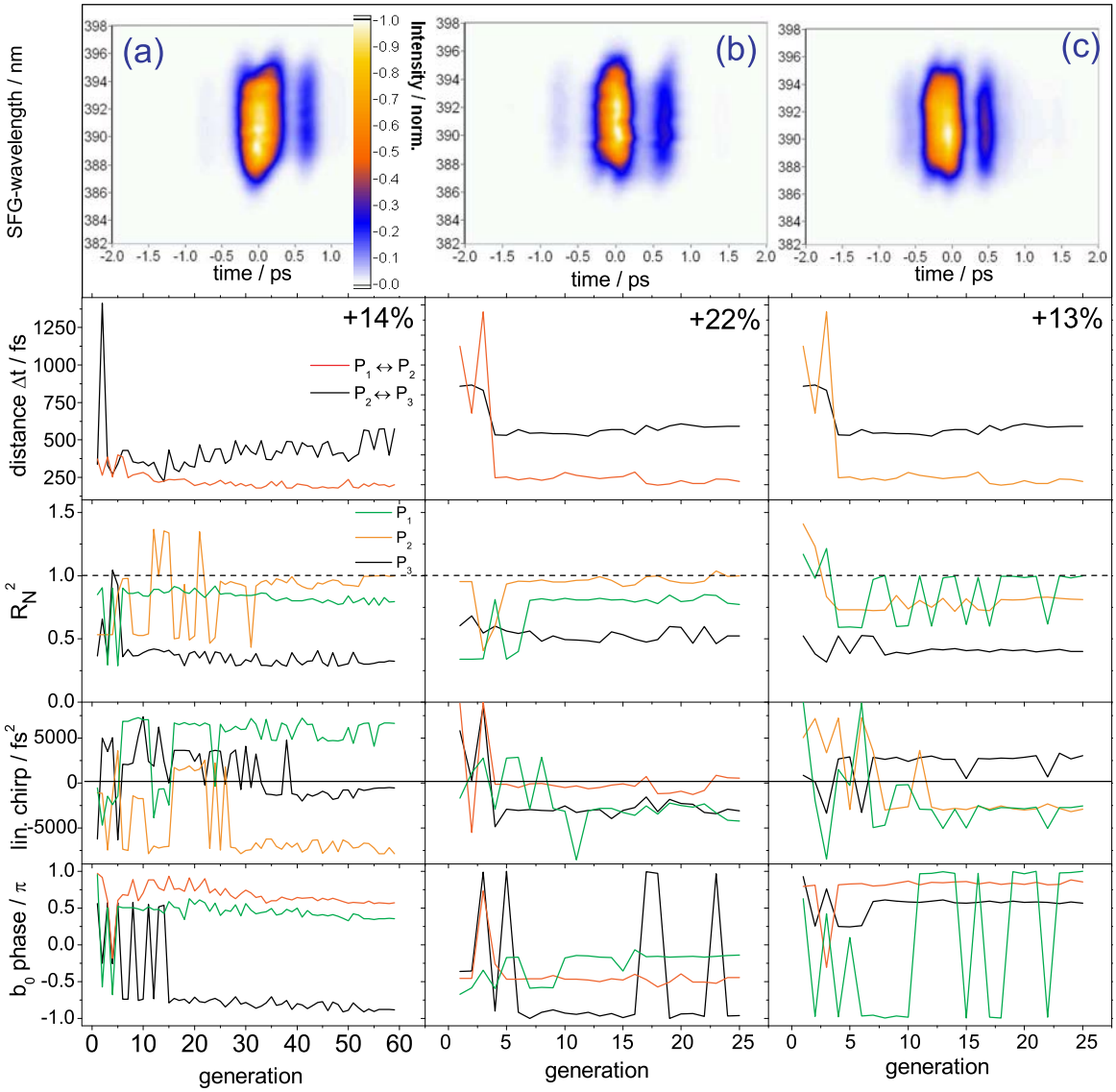

Figure 6.8: Course analysis for three, parametric optimization runs, maximizing the NaK ion yield using a three-sub pulse encoding. The upper row are the resulting XFROGs, the next rows (top to bottom) depict the development of sub pulse distance, energy, linear chirp, and b_0.

final pulse distances are found within the first few generations and stay more or less constant until the end. In the third row, the sub pulse energy ratios are plotted versus generation. For a comparison of results, they can be normalized to the final value of the highest energy ratio[12] (dashed horizontal line). For the (a) and (b) case, the energies develop similarly and parallel to each other. The high amount of fluctuation at the beginning of the (a) case can be also seen in the next row, which displays the evolution of the linear chirp. The linear chirp featured different results for all runs, case (b) shows the least amount of chirp, followed by (c). Pulse (a) shows symmetrically chirped sub pulses of approx. $\pm$ 6500 fs^2 (which is also indicated in the XFROG). The small resulting chirps ($\pm$ 20000 fs^2 were allowed) and the different results in numbers, but small in effect (as seen in the XFROGs) indicate a less pronounced importance of chirps for the ion yield. The zero order phase development is shown in the last row and, qualitatively, shows stable phase differences throughout the optimization, except for the first few generations (phase jumps of 2π can be discarded).

From the three pulse forms, an estimate of the induced wavepacket dynamics can be provided. The tiny sub pulse at the front is an unintended side pulse (from phase-only shaping) and causes a small population transfer to the first excited $A(2)^1\Sigma^+$ state. After about 1.5 oscillation periods, the wavepacket is located at the outer turning point, when the first of the two main sub pulses arrives and ionizes the molecule, and additionally, transfers more population from the ground state, which is again brought to the ionic state by the following main pulse after 220 fs at the outer turning point. After 650 fs, the last major pulse arrives and ionizes the population previously created by the first of the central double pulse.

To summarize, the three-pulse parametrization showed a greatly improved convergence speed compared to the free optimization experiments, with reproducible results in shape, however different in optimization factor, demonstrating the sensitivity of this particular experiment to small changes in pulse shape.

6.3.6 Six-pulse NaK optimization

Presented next is a step towards free optimization using a six-pulse-parametrization in a 23-dimensional search space. With constraints otherwise the same as for the three-pulse-parametrization, in a sense, a different "question" is asked to the experiment, which is to find an optimized waveform while enjoying a higher degree of freedom.

Fig. 6.7 (b) shows the result for the six-pulse parametrization (straight line) which offered an increased optimization factor of +54%, which is quite close to the results from free phase optimization which featured a 60% increase, consistent with results from Ref. [77] at this wavelength. By comparing the six-pulse parameterization to the free optimization result, a great deal of congruence can be made out in shape and optimization factor.

The six-pulse optimization shows a higher ionization efficiency than the three-pulse experiment, interestingly, all sub pulse distances amount to approximately 650 fs. Based on these results, a ladder-climbing scheme can be proposed, supported by

[12] as the sub pulses originate from a phase-only experiment

theoretical calculations[13]. This work draws a comparison of theoretically and experimentally optimized pulses, it concludes that the "later" pulses have a significant impact on the population of the ionic states due to additional wavepacket propagation of the intermediate $B(3)^1\Pi$ state, which likely yields the better optimization factors. The "convergence" of the six-pulse parametrization to the results of free, much more flexible, optimization demonstrates the potentiality of the introduced method which allows to gain knowledge about the treated systems by gradually increasing the complexity of the search strategy.

6.4 Spectral parametrization

Implementing a "peak finder" follows a similar motivation as pulse cleaning from Chapter 4. It is a somewhat complementary approach; cleaning removes unnecessary structures from the spectral domain whereas the peak finder searches for the most relevant spectral features "from scratch".

The peak finder algorithm essentially consists of a spectral parametrization with a problem-adapted encoding which accounts for the spectral particularities observed for free optimization. One of them is the early convergence of spectral peaks observed in the course analysis of free optimization (Chapter 5). As there was no special operator employed to sweep genetic information (such as spectral peaks) across the genome[14] more variety to the probed frequencies could be introduced by a different parameterization.

The introduced peak finder algorithm parametrizes the transmission $T(\omega)$ in a way that L multiple Gaussian peaks are steered by the algorithm, with a spectral encoding

$$\vec{x} = \left\{T_1, \delta\lambda_1, \Delta\lambda_1, \cdots, T_L, \delta\lambda_L, \Delta\lambda_L\right\}. \tag{6.17}$$

Each peak l consists of three parameters, transmission T_l, FWHM width $\delta\lambda_l$ (with a minimal width of the pixel resolution), and distance to the central wavelength $\Delta\lambda_l$. All other transmissions are set to zero, resulting in a search space dimension of $3 \times L$ for the amplitude-only case, when a free phase optimization is incorporated, this number becomes $3 \times L + N$.

6.4.1 Transition peak finder for NaK

For the first experiment on NaK, an amplitude-only encoding is chosen (meaning a flat phase filter) in order to identify the otherwise precluded vibronic pathways[15]. Amplitude modulated pulses are time-symmetric and usually consist of a main peak with smaller side pulses.

Fig. 6.9 (a) displays the obtained pulse spectrum after a run of the peak finder algorithm in amplitude-only mode. Several of the original eleven Gaussian peaks (33 parameters) conglomerate to a broader peak around the central wavelength

[13] at a wavelength of 770 nm [79]

[14] operators which intentionally induce such cross-gene interactions are sometimes called "creep" [93] or "copy mutate" [36]

[15] as argued in Chapter 4

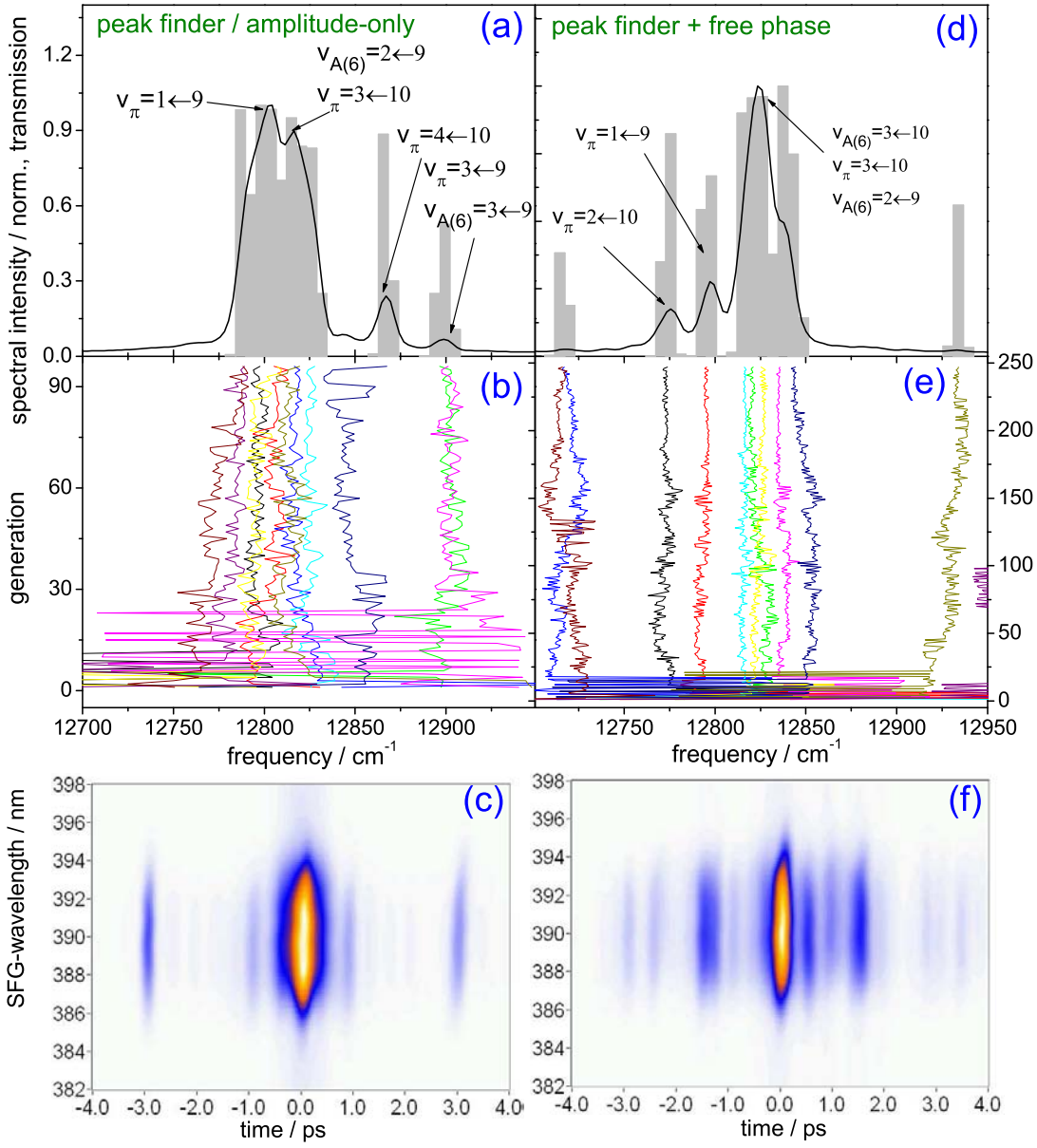

Figure 6.9: Transition finder applied on NaK ionization with a flat phase (left column) and with an additional free phase (optimization), shown in the right column. Graph (a) and (d) show the resulting spectra including the identified transitions, (b) and (e) are optimization courses for the peak central frequencies, while (c) and (f) depict the XFROG traces of the optimized pulses.

around 12820 cm^{-1}, and there are two single peaks at 12867 cm^{-1} and 12899 cm^{-1}. Both $A(6)^1\Sigma^+ \leftarrow A(2)^1\Sigma^+$ and $B(3)^1\Pi \leftarrow A(2)^1\Sigma^+$ transition frequencies can be identified. To observe how the spectral parametrization works, the parameter course is plotted in Fig. 6.9 (b). There, the development of the peak wavelength $\Delta\lambda_l$ versus generation (from bottom to top) is shown, whereby a convergence towards the final result (a) can be seen at the upper end. The initial chaos lasts for 25 generations, from then on, only a slow adaptation to the final values is observed, except for the 12867 cm^{-1} line, which shows an "undecided" behavior and can be treated as such when interpreting this particular spectral line. The result in the time domain (c) shows a structure with a major central peak and symmetrical, vanishing side pulses. The transition to the ionic state is most likely to be found at the inner turning point in a direct three-photonic process, due to the hindered temporal evolution (with only faint side pulses at approx. ± 3 and ± 1 ps).

Peak finder/free phase. To evaluate the interplay of amplitude and phase with this particular kind of parametrization, in another experiment, the phase was allowed to freely evolve, permitting a temporal waveform expansion.

Fig. 6.9 (d) displays the resulting spectrum. Except for the central structure around 12825 cm^{-1}, different transition frequencies can be found, compared to the amplitude-only case, which can easily be ascribed to the incipient wavepacket dynamics which can now utilize the outer turning point of the $A(2)^1\Sigma^+$ state and its favorable Franck-Condon window [133]. The parameter course (e) shows an uniform evolution from generation 23 on, with only slight changes until the final result is reached. The increased convergence time compared to the amplitude-only case is attributed to the additional free phase modulation. The XFROG (f) shows a more extended and more complex temporal pulse structure.

6.4.2 NaK isotope selective ionization

The next experiments using the peak finder will be isotope selective ionization for the NaK molecule. Studies of free optimization experiments on isotope selective ionization on $^{23}Na^{39}K$ / $^{23}Na^{41}K$ molecules are available in Refs. [80, 134], including a joint theoretical/experimental study [110]. Here, results from parametric optimization will be presented and discussed. The motivation to employ the peak finder algorithm for wavepacket isotope separation are the highly structured frequency patterns which were regularly observed. For isotope selective optimization of NaK, different premises apply as for the $^{39,39}K_2$ / $^{39,41}K_2$ system [89, 101]. The main differences to the potassium dimer lies in the resonant, intermediate potential energy surfaces and their isotope shifts. For K_2, two equal potentials are involved to obtain a high selectivity; NaK on the other hand features two potentials at approximately the same energy, namely $A(6)^1\Sigma^+$ and $B(3)^1\Pi$. Transitions via the $B(3)^1\Pi$ state are favorable at the outer turning point due to Franck-Condon factors and resonance conditions, whereas for the $A(6)^1\Sigma^+$ state, ionization may occur also at smaller nuclear distances [81].

The frequency shift of the shown transitions between the isotopes (see the double lines in Fig. 6.10 on the right) is about -7 cm^{-1} and increases for higher energies [112, 80], which is approximately the employed shaper resolution of the SLM-256.

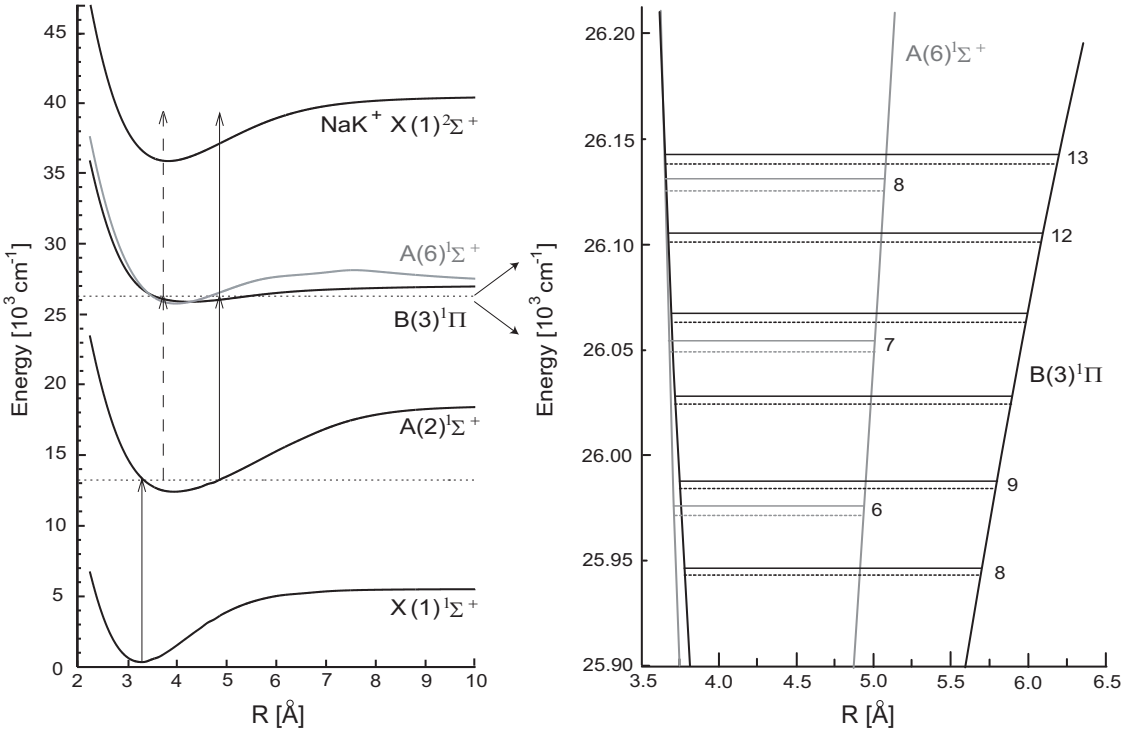

Figure 6.10: Potential curves for NaK (taken from Ref. [78]), including an excerpt (right) which highlights the energy spacing of the vibrational states of two most abundant isotopes of the $B(3)^1\Pi$ and $A(6)^1\Sigma^+$ potentials (taken from Ref. [112]).

The peak finder will be used to increase the ratio of the lighter isotope versus the heavier isotope, starting with the regular isotope ratio of an unshaped pulse (in the beam) of about 13.6:1.

6.4.3 Peak finder / NaK isotopes

At a wavelength of 780 nm, amplitude-only and phase- and amplitude isotope ratio maximizations were carried out in order to compare parametric optimizations with the peak finder with the results from free optimization.

Amplitude-only. Fig. 6.11 (a) and (b) compares the results from free amplitude-only ($^{39,39}K_2$ / $^{39,41}K_2$ ratio of 28:1) to parametric amplitude-only (20:1) measurements. The differences, two additional major peaks for the free optimization and its higher factor have to be contributed to the high amount of experimental noise which is even more critical as a ratio of two noisy signals is taken. It requires repeated runs to determine the highest possible optimization factor and to obtain a reliable result[16]. An association of peaks to vibrational transitions of different electronic states is possible, whereby the most distinct peak around 12825 cm^{-1} corresponds to three transitions within its frequency range, namely the $A(6)^1\Sigma^+$ ($3 \leftarrow 10$ and $2 \leftarrow 9$) and $B(3)^1\Pi$ ($3 \leftarrow 10$) transitions. Another side peak is located at approx. 12900 cm^{-1} and can be ascribed to other transitions. Although there are no perfect

[16] as shown for the three spectra in Fig. 6.11 (d)

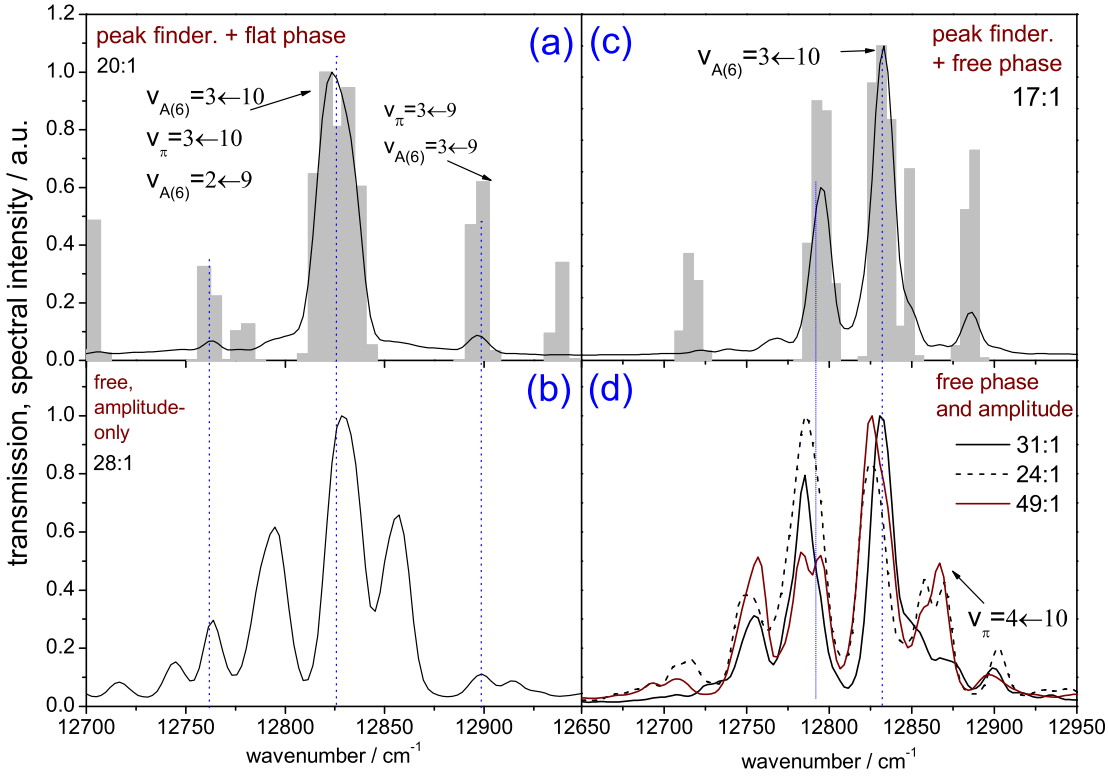

Figure 6.11: Transition finder algorithm, applied on NaK isotope selective optimization. (a) and (b) were performed with amplitude-only modulation, (c) and (d) used phase- and amplitude modulation. The numbers below the optimization types are the optimization factors, the dashed vertical lines indicate corresponding transitions found by the differing methods.

matches, the parametrization case, in any way, manages to increase the isotope ratio with a less complicated spectral structure than the free optimization.

Phase and amplitude. Graphs (c) and (d) were recorded using combined phase and amplitude modulation. There is a good agreement of the major features which consist of the two central peaks (marked by the vertical dashed lines), while having considerably lower factors, closely above the isotope ratio of an unshaped pulse. In (d), three subsequent experiments with different spectral results from phase and amplitude measurements were overlaid to provide an insight to the reproducibility of the experiments. They exhibit substantially different temporal structures, but still agree to a large part in the spectral domain, which highlights the difficulties and ambiguities the algorithm has to face in the highly noisy environment. The two most prominent features (at 12790 cm^{-1} and 12830 cm^{-1}) are also detected by the peak finder, whereby one of them could be assigned to the $A(6)^1\Sigma^+$ $(3 \leftarrow 10)$ transition.

6.5 Summary

The aim of this chapter was to introduce and test new parametrizations on molecular systems, presenting them as tools for investigating molecular dynamics. The improved convergence speed together with customized and physically motivated parameters helped enquiring the (isotope selective) ionization of the NaK molecule with femtosecond pulses under different constraints. A comparison with results from free optimization showed a gradual convergence in yield and shape for the single isotope (three-pulse→six-pulse→free optimization).

The temporal parametrization, unlike other encodings from the literature, allows unsymmetrical pulse forms, customized restrictions and boundary conditions which can be chosen by physically relevant criteria. Apart from the expanded shaping capabilities, say, versus sine-parametrization, also a more distinguished experimental profile can be incorporated; asking the experiment specific questions, which the feedback loop tries to answer by finding the optimal Hamiltonian. The spectral parameterization was able to locate relevant transition frequencies in only a matter of a few generations.